

Low-rank Random Tensor for Bilinear Pooling

Yan Zhang^{†‡} Krikamol Muandet[†] Qianli Ma[†] Heiko Neumann[‡] Siyu Tang^{†§}

[†]Max Planck Institute for Intelligent Systems, Tübingen, Germany

[‡]Institute of Neural Information Processing, Ulm University, Germany

[§]University of Tübingen, Tübingen, Germany

{yan.zhang,krikamol,qianli.ma,stang}@tuebingen.mpg.de

{yan.zhang,heiko.neumann}@uni-ulm.de

Abstract

Bilinear pooling is capable of extracting high-order information from data, which makes it suitable for fine-grained visual understanding and information fusion. Despite their effectiveness in various applications, bilinear models with massive number of parameters can easily suffer from curse of dimensionality and intractable computation. In this paper, we propose a novel bilinear model based on low-rank random tensors. The key idea is to effectively combine low-rank tensor decomposition and random projection to reduce the number of parameters while preserving the model representativeness. From the theoretical perspective, we prove that our bilinear model with random tensors can estimate feature maps to reproducing kernel Hilbert spaces (RKHSs) with compositional kernels, grounding the high-dimensional feature fusion with theoretical foundations. From the application perspective, our low-rank tensor operation is lightweight, and can be integrated into standard neural network architectures to enable high-order information fusion. We perform extensive experiments to show that the use of our model leads to state-of-the-art performance on several challenging fine-grained action parsing benchmarks.

1 Introduction

Bilinear pooling is an effective operation to extract second-order information from features, to calculate feature channel interactions and to perform feature aggregation across different spatial regions, temporal durations or modalities. Therefore, it has been successfully employed in various computer vision tasks, such as fine-grained image classification [1, 2, 3, 4, 5, 6], human action analysis [7, 8, 9, 10], visual question answering [11, 12, 13, 14] and so forth.

It is reported in the literature that second-order information is beneficial for large-scale visual tasks [2, 10], and extracting such information usually requires a bilinear model. Specifically, given two generic feature vectors $\mathbf{x} \in \mathbb{R}^{D_X}$ and $\mathbf{y} \in \mathbb{R}^{D_Y}$, the bilinear model based on high-order tensor multiplication [12, Eq. (2)] is given by:

$$\mathbf{z} = \mathcal{T} \times_1 \mathbf{x} \times_2 \mathbf{y}, \quad (1)$$

where $\mathcal{T} \in \mathbb{R}^{D_X \times D_Y \times D_Z}$ is a three-way tensor, and the operations \times_1 and \times_2 are the mode-1 and mode-2 multiplication, respectively. The tensor \mathcal{T} determines how information in the output $\mathbf{z} \in \mathbb{R}^{D_Z}$ is constructed from interactions between the elements in \mathbf{x} and \mathbf{y} . Though being a powerful scheme for information fusion, such model tends to suffer from *curse of dimensionality* and *intractable computation* [15]. Specifically, $\text{dim}(\mathcal{T})$ grows exponentially with the number of available channels. For the bilinear models in Eq. (1), the number of free parameters grows cubically $\mathcal{O}(D_X D_Y D_Z)$ with respect to feature dimensions, which is prohibitive even for moderate number of features, hence limiting the representation power of the model.

A common approach to reduce the number of parameters is to impose specific assumptions on the structure of \mathcal{T} in Eq. (1). For example, when $D_X = D_Y = D_Z = D$ and \mathcal{T} is a three-way identity tensor, we simply have $\mathbf{z} = \mathbf{x} \circ \mathbf{y}$ with \circ being the Hadamard product (element-wise product). When the mode-3 matricization of \mathcal{T} is an identity matrix of size $D_X D_Y$, we have $\mathbf{z} = \text{vec}(\mathbf{x} \otimes \mathbf{y})$, i.e., the vectorization of the outer product between the two input features. Alternatively, another common approach in the literature such as [16, 12, 4] is to perform low-rank decomposition of \mathcal{T} , and then learn the parameters in individual components. These approaches reduce the model parameters considerably at the cost of lowering the model representativeness.

In this paper, we introduce a new type of bilinear model by effectively combining low-rank tensor decomposition and random projection. Our model can significantly reduce the number of parameters via an assumption that each frontal slice of \mathcal{T} , but not \mathcal{T} itself, is a low-rank matrix. Rather than first lifting the feature dimension and then performing Hadamard product as proposed in [16, 12], we first reduce the feature dimension and then performing outer product. As a result, our method reduces the runtime complexity from $\mathcal{O}(Dd + d)$ to $\mathcal{O}(D\sqrt{d} + d)$, and space complexity from $\mathcal{O}(Dd)$ to $\mathcal{O}(D\sqrt{d})$, with D and d being the input and output feature dimension, respectively. Consequently, the resulting bilinear operation is lightweight and can be plugged into large deep neural networks in an efficient manner.

Decreasing the number of parameters has the risk of reducing the model capacity, hence losing the capability of capturing complex structures in the data. We overcome this issue by exploring the idea of random projection. We project feature vectors with random matrices that are sampled from certain distributions. The key insight here is that, when the parameters of the bilinear model are sampled with different underlying distributions, the model can approximate feature maps of different kernels, leading to different model capacities. We find that, when the model parameters are sampled from Rademacher distribution, the bilinear model can approximate the multiplication of linear kernels. When the model parameters are sampled from Gaussian distribution with orthogonality constraints, the bilinear model can approximate multiplication of Gaussian kernels. Thus, by choosing random matrices from specific distributions, we can explicitly manipulate the model capacity without sacrificing the computation efficiency. Moreover, our theoretical findings provide us with straightforward insights on how to choose model hyper-parameters and how to combine with other layers in a deep neural network.

We summarize our contributions as follows:

- We propose a novel bilinear model with a random three-way tensor. Via low-rank decomposition of each frontal slice, our method significantly reduces the parameter amount of the bilinear model, and hence can serve as a computationally efficient feature fusion operation.
- Based on different underlying distributions, we prove that the proposed random tensors can estimate the feature maps to reproducing kernel Hilbert spaces (RKHSs) with different compositional kernels.
- We combine our method with the state-of-the-art multi-stage deep neural network for action segmentation and produce superior results.

Our paper is organized as follows. First, we discuss related work in Section 2. Next, we present our contribution in Section 3, followed by the experimental results in Section 4. Finally, we conclude the paper and discuss possibilities for future directions in Section 5.

2 Related Work

Low-rank approximation. There exist many investigations on low-rank tensor decomposition for bilinear pooling. The work of multi-modal low-rank bilinear pooling [16] assumes that each frontal slice of the three-way tensor can be decomposed into two low-rank matrices, and the fusion of the two input features can then be realized by matrix multiplication and Hadamard product. The work of [17] introduces more operations after the low-rank bilinear pooling [16] such as dropout, power normalization, L2 normalization and so forth, so as to improve the performance of visual question answering (VQA). The work of [12] uses the form of tensor Tucker decomposition, producing three matrices and a smaller core three-way tensor. To introduce sparsity, each frontal slice of the core tensor is assumed to be rank- R .

Explicit feature maps of kernels. Approximating nonlinear kernels with approximate feature maps has many benefits for large-scale training, e.g., avoiding computing Gram matrix for all training data. The work of [18] uses binary random entries to approximate inner product kernels, especially the p -th order polynomial kernels. The work of [19] and [20] uses tensor sketch technique to approximate polynomial kernels, which has lower approximation error bound but higher computational cost. The work of [21] uses orthogonal random features to approximate feature maps of Gaussian kernels. To boost the computational speed, a structured version with normalized Walsh-Hadamard matrices is proposed.

Our method is inspired by the above two research fields. To reduce the model complexity, referring to [16, 12] we assume each frontal slice of the three-way tensor is a rank- R matrix. In contrast to using element-wise product as in other works, we use vector outer product to incorporate correlations across different feature channels. To guarantee the model representativeness, we use random projection to approximate explicit feature maps of kernel compositions. Comparing with learnable matrices in other studies, our method clearly shows that the resulting vector locates within certain RKHS, and hence we can manipulate the model capacity straightforwardly.

3 Method

3.1 Tensor frontal low-rank approximation

Here we follow the tensor notations in [22]. Eq. (1) can be re-written in terms of matrix-vector multiplication as

$$\mathbf{z} = \mathbf{T}_{(3)} \text{vec}(\mathbf{x} \otimes \mathbf{y}), \quad (2)$$

where $\mathbf{T}_{(3)}$ is the mode-3 matricization of \mathcal{T} , $\text{vec}(\cdot)$ denotes column-wise vectorization of a matrix, and \otimes denotes vector outer product. In other words, the bilinear operation in Eq. (1) is equivalent to first computing the correlation matrix between the two features and then performing linear projection.

It follows from Eq. (2) that each entry of the output feature vector \mathbf{z} is a weighted sum of all the entries in the correlation matrix $\mathbf{x} \otimes \mathbf{y}$, i.e.,

$$z_k = \langle \text{vec}(\mathcal{T}[:, :, k]), \text{vec}(\mathbf{x} \otimes \mathbf{y}) \rangle = \sum_{i=1}^{D_X} \sum_{j=1}^{D_Y} \mathcal{T}[i, j, k] v_{f(i, j)}, \quad (3)$$

where $\mathbf{v} := \text{vec}(\mathbf{x} \otimes \mathbf{y})$. If the frontal matrix $\mathcal{T}[:, :, k]$ is a rank-one matrix, i.e., $\mathcal{T}[:, :, k] = \mathbf{e} \otimes \mathbf{f}$ for some $\mathbf{e} \in \mathbb{R}^{D_X}$ and $\mathbf{f} \in \mathbb{R}^{D_Y}$, then we can rewrite Eq. (3) as $z_k = \langle \text{vec}(\mathbf{e} \otimes \mathbf{f}), \text{vec}(\mathbf{x} \otimes \mathbf{y}) \rangle = \langle \mathbf{e}, \mathbf{x} \rangle \langle \mathbf{f}, \mathbf{y} \rangle$.

Thus, we define the projection matrices $\mathbf{E} = [\mathbf{e}_1, \mathbf{e}_2, \dots, \mathbf{e}_M]^T$ and $\mathbf{F} = [\mathbf{f}_1, \mathbf{f}_2, \dots, \mathbf{f}_N]^T$ for two sets of vectors $\{\mathbf{e}_i\}_{i=1}^M \subset \mathcal{X}$ and $\{\mathbf{f}_j\}_{j=1}^N \subset \mathcal{Y}$ with $M \leq D_X$ and $N \leq D_Y$. Then, the fusion map $\phi : \mathbb{R}^{D_X} \times \mathbb{R}^{D_Y} \rightarrow \mathbb{R}^{MN}$ can be defined as

$$\mathbf{z} := \phi(\mathbf{x}, \mathbf{y}) = \text{vec}((\mathbf{E}\mathbf{x}) \otimes (\mathbf{F}\mathbf{y})). \quad (4)$$

If we assume further that $\mathcal{T}[:, :, k]$ is a rank- R matrix, i.e., $\mathcal{T}[:, :, k] = \sum_{r=1}^R \mathbf{e}_i^r \otimes \mathbf{f}_j^r$, we obtain

$$\mathbf{z} := \phi(\mathbf{x}, \mathbf{y}) = \text{vec} \left(\sum_{r=1}^R (\mathbf{E}^r \mathbf{x}) \otimes (\mathbf{F}^r \mathbf{y}) \right), \quad (5)$$

where $\mathbf{E}^r = [\mathbf{e}_1^r, \mathbf{e}_2^r, \dots, \mathbf{e}_M^r]^T$ and $\mathbf{F}^r = [\mathbf{f}_1^r, \mathbf{f}_2^r, \dots, \mathbf{f}_N^r]^T$ for $r = 1, 2, \dots, R$. With such low-rank assumption, we avoid computing the high-dimensional correlation matrix $\mathbf{x} \otimes \mathbf{y}$, which considerably reduces the model parameters from $D_X D_Y D_Z$ to $R(M D_X + N D_Y)$ with a small value of R .

Similar low-rank assumption is also used in [12, 16], in which the two input feature vectors are first projected to a common vector space and then fused via Hadamard product. Assuming the input feature vectors are of the same dimension D and the output feature vector is of dimension d , then such operation requires $\mathcal{O}(Dd + d)$ operations to compute and requires $\mathcal{O}(Dd)$ memory to store. In contrast, our method requires $\mathcal{O}(D\sqrt{d} + d)$ for computation and $\mathcal{O}(D\sqrt{d})$ for storage. Since in practice it normally requires more dimensions to represent a higher-order feature, i.e. $d \gg D$, our method has consistently better runtime (see Tab. 2) and hence is more suitable to be employed in a sophisticated deep neural net as a pooling layer.

3.2 Random projection

Since we have reduced a large number of model parameters via the low-rank assumption, we could lead to a risk of significantly reducing the model capacity, causing the model not being able to learn complex functions in large-scale tasks. Towards understanding the capacity of the bilinear model, we find that the parameter values (i.e. the matrix entries) defined in Eq. (4) and Eq. (5) can influence the capacity, without adding or removing learnable parameters, network layers, etc. Specifically, we randomly sample the parameters from certain distributions and perform random projection to explicitly manipulate the model capacity. Comparing with learning the bilinear model parameters via back-propagation, we have an explainable model to use in practice.

In what follows, we simplify the analyses by assuming that the rank $R = 1$ for ease of understanding. In our experiments, however, we can set the rank $R > 1$.

3.2.1 Rademacher random projection

Motivated by [18] and [19], we specify model parameters, i.e. the projection matrices \mathbf{E}^r and \mathbf{F}^r in the bilinear model (4) or (5) with random values sampled from Rademacher distribution. In this case, we show that the bilinear model given in Eq. (4) unbiasedly approximates a feature map to a reproducing kernel Hilbert space (RKHS), in which the associated kernel is the multiplication of two linear kernels in \mathcal{X} and \mathcal{Y} , respectively.

Theorem 1. *Let $\mathbf{E}^r \in \mathbb{R}^{M \times D_X}$ and $\mathbf{F}^r \in \mathbb{R}^{N \times D_Y}$ for any $r \in \{1, 2, \dots, R\}$ be Rademacher random matrices whose entries are determined by an independent Rademacher random variable $\sigma \in \{-1, 1\}$. For any $\mathbf{x}_1, \mathbf{x}_2 \in \mathcal{X}$ and $\mathbf{y}_1, \mathbf{y}_2 \in \mathcal{Y}$, let $\mathbf{z}_1 = \phi(\mathbf{x}_1, \mathbf{y}_1)$ and $\mathbf{z}_2 = \phi(\mathbf{x}_2, \mathbf{y}_2)$ be the output features given by the bilinear model in Eq. (4). Assume that $R = 1$ and define a kernel function by $k(\mathbf{z}_1, \mathbf{z}_2) = \langle \mathbf{z}_1, \mathbf{z}_2 \rangle$, then we have*

$$\mathbb{E}[k(\mathbf{z}_1, \mathbf{z}_2)] = MN \langle \mathbf{x}_1, \mathbf{x}_2 \rangle \langle \mathbf{y}_1, \mathbf{y}_2 \rangle.$$

Next, we characterize the error of such kernel approximation.

Corollary 1. *Let $\mathbf{z}_1, \mathbf{z}_2$, and $k(\mathbf{z}_1, \mathbf{z}_2)$ be defined as in Theorem 1. Then, the following inequality holds:*

$$\mathbb{P}(|k(\mathbf{z}_1, \mathbf{z}_2) - \mathbb{E}[k(\mathbf{z}_1, \mathbf{z}_2)]| > \epsilon) \leq 2 \exp \left(-\frac{\epsilon^2 MN}{2p^8 \tilde{R}^8} \right), \quad (6)$$

for some positive constants $p \geq 1$ and $\tilde{R} \geq 1$, which are independent of the feature dimension [18].

Their proofs are in Appendix A and B. In the case with rank $R > 1$, we also show that the bilinear model (5) approximates a feature map of a more complicated kernel composition (see Appendix A). To remove the effect of the scaling factors, we rewrite Eq. (5) as

$$\mathbf{z} = \phi(\mathbf{x}, \mathbf{y}) = \frac{1}{R\sqrt{MN}} \cdot \text{vec} \left(\sum_{r=1}^R (\mathbf{E}_r \mathbf{x}) \otimes (\mathbf{F}_r \mathbf{y}) \right). \quad (7)$$

Despite being able to deal with vector spaces with different dimensionalities, the drawback of the fusion map Eq. (4) or Eq. (7) as shown in Theorem 1 is that it can only capture second-order interactions between two features. Next, we consider an alternative way of constructing \mathbf{E}^r and \mathbf{F}^r using Gaussian random projection with orthogonal constraints [21].

3.2.2 Gaussian random projection.

Motivated by [21], we consider

$$\mathbf{E}^r = \frac{1}{\sigma^r} \mathbf{I}_{M \times D_X} \mathbf{R}^r \mathbf{P}^r, \quad \mathbf{F}^r = \frac{1}{\rho^r} \mathbf{I}_{N \times D_Y} \mathbf{S}^r \mathbf{Q}^r \quad \text{with } r = 1, 2, \dots, R, \quad (8)$$

where \mathbf{R}^r and \mathbf{S}^r are diagonal matrices with diagonal entries sampled i.i.d. from the chi-squared distributions $\chi^2(D_X)$ and $\chi^2(D_Y)$ with D_X and D_Y degrees of freedom, respectively, \mathbf{P}^r and \mathbf{Q}^r are uniformly distributed random orthogonal matrices¹, and $\mathbf{I}_{M \times D_X}$ and $\mathbf{I}_{N \times D_Y}$ are identity

¹Specifically, \mathbf{P}^r and \mathbf{Q}^r are uniformly distributed on the Stiefel manifold [21, 23].

matrices with the first M and N rows, respectively. Here, $\{\sigma^r\}_{r=1}^R$ and $\{\rho^r\}_{r=1}^R$ are bandwidth parameters. Then, the bilinear models (4) and (5) based on the projection matrices given in Eq. (8) are approximated feature maps to RKHSs with a product of Gaussian kernels. Especially, when the rank $R = 1$, such approximation is unbiased.

Theorem 2. *Let $\mathbf{E}^r \in \mathbb{R}^{M \times D_X}$ and $\mathbf{F}^r \in \mathbb{R}^{N \times D_Y}$ for any $r \in \{1, 2, \dots, R\}$ be random matrices whose entries are determined as in Eq. (8). For any $\mathbf{x}_1, \mathbf{x}_2 \in \mathcal{X}$ and $\mathbf{y}_1, \mathbf{y}_2 \in \mathcal{Y}$, let $\mathbf{z}_1 = \phi(\mathbf{x}_1, \mathbf{y}_1)$ and $\mathbf{z}_2 = \phi(\mathbf{x}_2, \mathbf{y}_2)$ be the output features given by the bilinear model in Eq. (5). Assume that $R = 1$ and define a kernel function by $k(\mathbf{z}_1, \mathbf{z}_2) = \langle \mathbf{z}_1, \mathbf{z}_2 \rangle$, then we have*

$$\mathbb{E}[k(\mathbf{z}_1, \mathbf{z}_2)] = \exp\left(-\frac{\|\mathbf{x}_1 - \mathbf{x}_2\|_2^2}{2\sigma_r^2}\right) \exp\left(-\frac{\|\mathbf{y}_1 - \mathbf{y}_2\|_2^2}{2\rho_r^2}\right). \quad (9)$$

Next, we characterize the variance of this inner product. For simplicity, we only present the result for $R = 1$.

Corollary 2. *Let $\mathbf{z}_1, \mathbf{z}_2$, and $k(\mathbf{z}_1, \mathbf{z}_2)$ be defined as in Theorem 2, as well as $R = 1$, $a_r = \|\mathbf{x}_1 - \mathbf{x}_2\|_2^2/\sigma_r^2$ and $b_r = \|\mathbf{y}_1 - \mathbf{y}_2\|_2^2/\rho_r^2$. Then there exists functions f and g such that*

$$\text{Var}(k(\mathbf{z}_1, \mathbf{z}_2)) \leq A \cdot B + A \cdot C + B \cdot D, \quad (10)$$

where

$$\begin{aligned} A &= \frac{1}{2M} \left[\left(\left(1 - e^{-a_r^2}\right)^2 - \frac{M-1}{D_X} e^{-a_r^2} a_r^4 \right) + \frac{f(a_r)}{D_X^2} \right], & C &= \left[\exp\left(-\frac{b_r^2}{2}\right) \right]^2 \\ B &= \frac{1}{2N} \left[\left(\left(1 - e^{-b_r^2}\right)^2 - \frac{N-1}{D_Y} e^{-b_r^2} b_r^4 \right) + \frac{g(b_r)}{D_Y^2} \right], & D &= \left[\exp\left(-\frac{a_r^2}{2}\right) \right]^2. \end{aligned}$$

One can see the proofs in Appendix C and D. In case of rank $R > 1$, we also show that the approximated kernel is composed in a more sophisticated manner. To remove the scaling effect, we rewrite the bilinear model (5) with the random matrices (8) as

$$\mathbf{z} = \phi(\mathbf{x}, \mathbf{y}) = \frac{1}{R} \cdot \text{vec} \left(\sum_{r=1}^R (\mathbf{E}_r \mathbf{x}) \otimes (\mathbf{F}_r \mathbf{y}) \right). \quad (11)$$

In our experiments, we use a simpler alternative version $\mathbf{E}^r = \frac{\sqrt{D_X}}{\sigma^r} \mathbf{I}_{M \times D_X} \mathbf{P}^r$ and $\mathbf{F}^r = \frac{\sqrt{D_Y}}{\rho^r} \mathbf{I}_{N \times D_Y} \mathbf{Q}^r$. Despite approximating the kernel biasedly [21, Theorem 2], such simplified version has very similar empirical behaviors to the original version, especially when the feature dimensionality is high. In addition, rather than regarding the Gaussian radii as hyper-parameters, we learn them via backpropagation when employing the bilinear model (11) as an intermediate layer in a deep neural net.

From the above theorems and corollaries we find that larger values of M and N , namely higher output feature dimension, can yield smaller error upper bounds. Therefore, it is encouraged to increase the values of M and N in practice for better kernel approximation. In addition, we can also increase the model complexity via increasing the rank R . Moreover, our theorems are based on the assumption of $M \leq D_X$ and $N \leq D_Y$. In fact, we can also first lift the feature dimension and perform vector outer product. Instead of setting $M > D_X$ and $N > D_Y$, we perform bilinear pooling several times with different random projection matrices, and then concatenate the output feature vectors. One can see the same operation in [21].

4 Experiments

We conduct experiments for the task of fine-grained temporal action segmentation, which aims at assigning each individual frame an action label. In such experiments, the two input features \mathbf{x} and \mathbf{y} in Eq. (7) and (11) are identical, and we set the same number of rows (i.e. $M = N$) to matrices \mathbf{E}^r and \mathbf{F}^r , $\forall r$. Consequently, there only remain two hyper-parameters in the bilinear model, i.e. the rank R and the number of rows N of matrices. Our experiments are two-fold: (i) To verify the effectiveness of our method, we use the temporal convolutional net (TCN) [24] due to its simple structure. We replace the max pooling in TCN by bilinear pooling as in [10]. (ii) To show how to use our method in practice, we propose a bilinear residual module to merge the first and second-order information, and combine it with the multi-stage temporal convolutional net (MS-TCN) [25] to yield state-of-the-art performance.

Datasets and evaluation metrics. We evaluate our method on the **50 Salads** [26] dataset and the **GTEA** [27, 28] dataset. For fair comparison, in our experiments with TCN we use the identical frame-wise features and temporal resolutions with [24]. Also, in our experiments with MS-TCN we use the identical frame-wise features and temporal resolutions with [25]. To evaluate the performance, we use the standard metrics, i.e. frame-wise accuracy, edit score and F1 scores with the IoU ratio of 0.1, 0.25 and 0.5 (F1@0.1, F1@0.25 and F1@0.5), respectively. One can see their detailed definitions in [24, 10, 25]. For brevity, we denote F1@0.1 as “F1 score” unless otherwise mentioned. Since each dataset has several splits, we report the results of cross-validation.

4.1 Action segmentation with TCN architecture.

We use the default architecture of TCN [24], which comprises an encoder and a decoder with symmetric modules. The convolutional layer in each individual encoder has 64 and 96 filters, respectively. We train the models using the Adam optimizer [29] with a fixed learning rate of 10^{-4} . Batch size is set to 8. The training process terminates after 300 epochs.

Ablation study. Here we investigate properties of our Rademacher random projection (RPBinary) and Gaussian random projection (RPGaussian). Fig. 1 shows the dependence of the model performance on ranks $R \in \{1, 2, 4, 8, 16\}$ and matrix rows $N \in \{1, 2, 4, 8\} \times \lceil \sqrt{D_X} \rceil$, with $D_X = 64$ in the first encoder and $D_X = 96$ in the second encoder. $[\cdot]$ is the operation to get the nearest integer. In this case the output feature dimension is then $\{1, 4, 16, 64\} \times D_X$. In all plots, the performance increases consistently with the matrix row N (hence the output feature dimension). This result is in line with Corollaries 1 and 2: larger values of M and N can yield lower variance upper bounds, hence better kernel approximation. In addition, increasing the rank cannot consistently yield better performance. Instead, an optimal rank value depends on the dataset and the applied bilinear model.

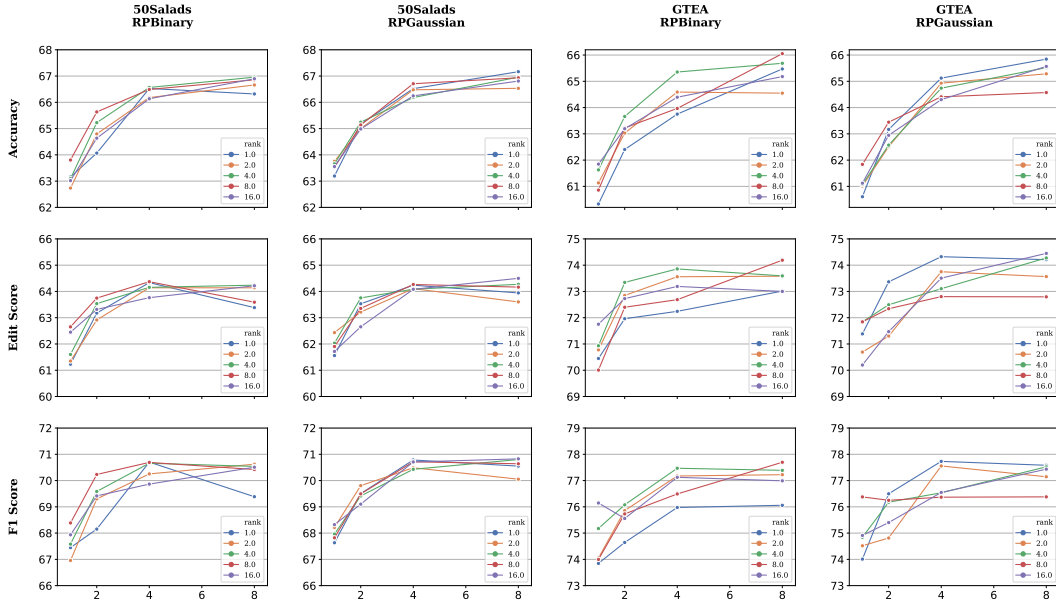


Figure 1: Ablation study: performance of our RPBinary and RPGaussian model, versus dimension / rank, on datasets **50Salads** and **GTEA**. In each plot, x-axis is the multiplier N on the number of matrix rows, y-axis is respective performance measure, and colors denote different ranks.

Comparison with other bilinear pooling methods. Here we compare our methods with two widely used bilinear pooling methods, i.e., [19] and [16]. The results are shown in Tab. 1. In this experiment, we set rank $R = 1$ and $N = D_X/2$ for both RPBinary and RPGaussian. To vary the output dimension, we perform our random projection-based pooling several times and concatenate the results. For fair comparison with other pooling methods, we use the same output feature dimensions as RPBinary and RPGaussian for each setting. Moreover, we repeat the experiment 3 times and report the result with the highest sum of the three metrics.

Table 1: Comparison with different bilinear pooling methods in terms of *accuracy/edit score/F1 score*. #components denotes the number of components in the concatenated output feature and only applies for our methods. The number in the parenthesis after the component denotes the output feature dimension of the first bilinear pooling module. For each metric and each setting, the best result is in boldface.

# components	50Salads			GTEA		
	1 (1024)	2 (2048)	4 (4096)	1 (1024)	2 (2048)	4 (4096)
Low-rank [16]	67.7 /64.4/71.5	68.6 / 66.4 /71.7	67.3/64.4/70.8	66.0/ 76.6 /79.0	65.6/74.7/78.6	66.8 /75.6/79.2
Compact [19]	67.2/65.8/71.7	66.9/65.6/71.7	67.0/65.9/ 71.9	65.9/75.3/78.1	67.0/74.9/79.1	65.8/75.3/ 79.9
Ours (Learnable)	66.4/65.0/70.5	67.2/65.1/71.3	66.8/ 66.4 /71.2	64.8/74.0/77.5	66.7/74.6/78.2	65.1/75.6/77.9
Ours (Binary)	66.0/ 65.9 /70.9	67.0/64.5/70.6	67.5 /64.9/71.3	65.2/73.2/77.0	68.6 / 76.1 / 80.2	65.4/76.6/78.0
Ours (Gaussian)	67.6/65.2/ 72.9	66.5/64.6/ 71.8	67.1/64.8/71.2	66.9 /76.5/ 79.8	66.9/75.8/78.7	65.9/ 76.8 /77.3

Table 2: Comparison of average per-batch (batch size = 8) run time, in millisecond. The number in the parenthesis after the component denotes the output feature dimension of the first bilinear pooling module. The fastest results are highlighted in boldface.

# components	50Salads			GTEA		
	1 (1024)	2 (2048)	4 (4096)	1 (1024)	2 (2048)	4 (4096)
Compact [19]	95.9	199.3	384.8	120.2	182.8	331.6
Low-rank [16]	83.8	157.8	304.0	83.6	166.5	314.4
Ours (Gaussian)	68.9	151.5	295.9	74.2	154.0	307.0

The comparison in terms of runtime is presented in Tab. 2. Since RPGaussian and RPBinary has the same complexity, we only show the results with RPGaussian. The runtime is per-batch (batch size=8) and is the averaged result after training with the first split for 300 epochs for each dataset.

According to Tab. 1 and Tab. 2, one can see that our bilinear pooling methods have comparable performances with the two baseline methods but with faster speed. This result indicates that our methods gain higher computational speed without sacrificing the model representation capability. In addition, the random projection in most cases outperforms the learnable counterpart, which indicates that approximating kernels can bring more stable performance than learning via back-propagation, and the associated RKHSs are likely to provide certain regularization.

4.2 Action segmentation with MS-TCN net.

Here, we demonstrate how to effectively incorporate our model into the state-of-the-art action parsing network (MS-TCN [25]) to produce superior performance.

Implementation Details. Based on our previous experiment results, we set rank $R = 4$ and $N = D_X/2$ ($D_X = 64$ as in [25]) for our bilinear model. Furthermore, we propose a bilinear residual module to merge the first and the second-order information, as illustrated in Fig. 2. First, we use bilinear pooling to extract the second-order information, and then use a regularized power normalization [10] to densify the feature and use channel-wise max normalization to re-scale the feature value [24]. Afterwards, we use a convolution layer to reduce the feature dimension to the number of classes. Since the second-order information tends to partition an action into smaller segments [10, Fig. 1], we use a larger convolution receptive field 25 according to [24]. To prevent overfitting we use a dropout layer, and then we compute the average between the first-order information and the second-order information.

Our bilinear residual module is applied at the end of each single stage of MS-TCN. To conduct fair comparison with the baseline MS-TCN model, we keep other model configurations and the loss function (including the hyper-parameters) unchanged. Similarly to the training scheme of MS-TCN [25], we use Adam [29] optimizer with learning rate of 0.0005, and the batch size is set to 1. Without direct mentioning, the training process terminates after 50 epochs.

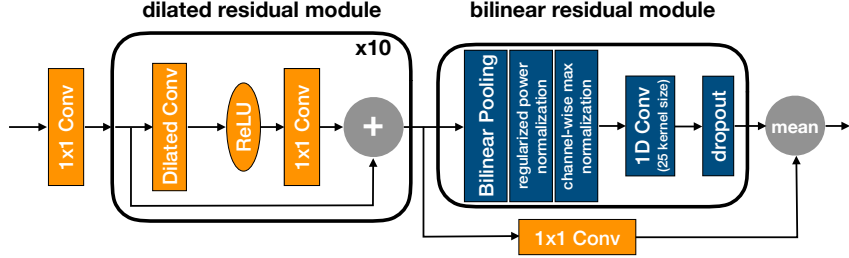


Figure 2: Illustration of combining MS-TCN and our bilinear pooling method.

Table 3: Influence of the dropout ratio tested on **50Salads**. Best results are in boldface.

dropout ratio	RPBinary					RPGaussian				
	acc.	edit	F1@0.1	F1@0.25	F1@0.5	acc.	edit	F1@0.1	F1@0.25	F1@0.5
0	77.4	62.8	71.0	68.1	59.1	78.0	62.0	70.0	67.4	57.6
0.5	79.4	68.8	76.8	73.9	63.8	75.6	66.6	73.5	68.6	58.7
0.7 (70 epochs)	79.9	70.7	78.0	75.2	65.4	80.6	71.0	78.4	75.8	66.7

Result. First, we find that the dropout ratio considerably influence the performance. Since the output feature dimension of bilinear pooling is 1024, the consecutive convolution layer has a large number of learnable parameters, causing the model prone to overfitting. The dropout influence is shown in Tab. 3. First, one can see that increasing the dropout ratio consistently improves the performance of both bilinear pooling methods, indicating that the overfitting problem is mainly caused by massive number of parameters in the consecutive convolutional layer. Second, with the dropout ratio of 0.7, RPGaussian outperforms RPBinary, which indicate that RPGaussian has more powerful representability. This fact can verify our theory that approximating a Gaussian kernel leads to higher model capacity than approximating a linear kernel.

In the end, we compare our method with several state-of-the-art methods on action segmentation. As shown in Tab. 4, for the **50Salads** dataset we report the results of RPGaussian and RPBinary with the dropout ratio 0.7 and 70 epochs. For the dataset **GTEA**, RPGaussian and RPBinary are associated with the dropout ratio 0.5 and 50 epochs. Our model consistently outperforms the state-of-the-arts, validating the effectiveness of the proposed bilinear model.

Table 4: Comparison with other network architectures on temporal action segmentation. The best results are in boldface.

	50 Salads					GTEA				
	Acc.	Edit	F1@0.1	F1@0.25	F1@0.5	Acc.	Edit	F1@0.1	F1@0.25	F1@0.5
TCN [24]	64.7	59.8	68.0	63.9	52.6	64.0	-	72.2	69.3	56.0
TDRN [30]	68.1	66.0	72.9	68.5	57.2	70.1	74.1	79.2	74.4	62.7
MS-TCN [25]	80.7	67.9	76.3	74.0	64.5	76.3	79.0	85.8	83.4	69.8
Ours(RPBinary)	79.9	70.7	78.0	75.2	65.4	77.1	81.4	86.5	84.5	71.7
Ours(RPGaussian)	80.6	71.0	78.4	75.8	66.7	77.2	82.3	86.7	84.3	72.7

5 Conclusion

In this work, we propose a novel bilinear model for fusing high-dimensional features. To reduce the number of model parameters, we utilize low-rank tensor decomposition. Instead of using element-wise product as in other works, we use the outer product of the features to model the high-order correlations among feature channels. To enrich the model representativeness while retaining the number of parameters, we use random projection to approximate feature maps to reproducing kernel Hilbert spaces with kernel compositions. To validate the effectiveness of our method, we perform extensive experiments on the action segmentation task, and have achieved state-of-the-art performance on challenging benchmarks. Our bilinear pooling operation is lightweight, easy to use, and can serve as a natural tool for fine-grained visual understanding and information fusion. In the future we will apply our methods on other tasks such as audio-video fusion and visual question answering.

Acknowledgement

Y. Zhang, Q. Ma and S. Tang acknowledge funding by Deutsche Forschungsgemeinschaft (DFG, German Research Foundation) Projektnummer 276693517 SFB 1233.

References

- [1] Joao Carreira, Rui Caseiro, Jorge Batista, and Cristian Sminchisescu. Semantic segmentation with second-order pooling. In *European Conference on Computer Vision*, pages 430–443. Springer, 2012.
- [2] Peihua Li, Jiangtao Xie, Qilong Wang, and Wangmeng Zuo. Is second-order information helpful for large-scale visual recognition. In *IEEE international conference on computer vision (ICCV)*. IEEE, pages 2070–2078, 2017.
- [3] Tsung-Yu Lin, Aruni RoyChowdhury, and Subhransu Maji. Bilinear convolutional neural networks for fine-grained visual recognition. *IEEE transactions on pattern analysis and machine intelligence*, 40(6):1309–1322, 2018.
- [4] Shu Kong and Charless Fowlkes. Low-rank bilinear pooling for fine-grained classification. In *IEEE Conference on Computer Vision and Pattern Recognition (CVPR)*, pages 7025–7034. IEEE, 2017.
- [5] Chaojian Yu, Xinyi Zhao, Qi Zheng, Peng Zhang, and Xinge You. Hierarchical bilinear pooling for fine-grained visual recognition. In *European Conference on Computer Vision*, pages 595–610. Springer, 2018.
- [6] Piotr Koniusz, Fei Yan, Philippe-Henri Gosselin, and Krystian Mikolajczyk. Higher-order occurrence pooling for bags-of-words: Visual concept detection. *IEEE transactions on pattern analysis and machine intelligence*, 39(2):313–326, 2017.
- [7] C. Feichtenhofer, A. Pinz, and A. Zisserman. Convolutional two-stream network fusion for video action recognition. In *2016 IEEE Conference on Computer Vision and Pattern Recognition (CVPR)*, pages 1933–1941, 2016.
- [8] Rohit Girdhar and Deva Ramanan. Attentional pooling for action recognition. In *Advances in Neural Information Processing Systems*, pages 34–45, 2017.
- [9] Anoop Cherian, Piotr Koniusz, and Stephen Gould. Higher-order pooling of cnn features via kernel linearization for action recognition. In *IEEE Winter Conference on Applications of Computer Vision (WACV)*, pages 130–138. IEEE, 2017.
- [10] Yan Zhang, Siyu Tang, Krikamol Muandet, Christian Jarvers, and Heiko Neumann. Local temporal bilinear pooling for fine-grained action parsing. In *Proceedings IEEE Conf. on Computer Vision and Pattern Recognition (CVPR)*, June 2019.
- [11] Zhou Yu, Jun Yu, Chenchao Xiang, Jianping Fan, and Dacheng Tao. Beyond bilinear: Generalized multimodal factorized high-order pooling for visual question answering. *IEEE Transactions on Neural Networks and Learning Systems*, 29(12):5947–5959, 2018.
- [12] Hedi Ben-Younes, Rémi Cadene, Matthieu Cord, and Nicolas Thome. Mutan: Multimodal tucker fusion for visual question answering. In *Proceedings of the IEEE international conference on computer vision*, pages 2612–2620, 2017.
- [13] Jin-Hwa Kim, Jaehyun Jun, and Byoung-Tak Zhang. Bilinear Attention Networks. In *Advances in Neural Information Processing Systems 31*, pages 1571–1581, 2018.
- [14] Akira Fukui, Dong Huk Park, Daylen Yang, Anna Rohrbach, Trevor Darrell, and Marcus Rohrbach. Multimodal compact bilinear pooling for visual question answering and visual grounding. *arXiv:1606.01847*, 2016.
- [15] Richard E Bellman. *Adaptive control processes: a guided tour*, volume 2045. Princeton university press, 2015.
- [16] Jin-Hwa Kim, Kyoung-Woon On, Woosang Lim, Jeonghee Kim, Jung-Woo Ha, and Byoung-Tak Zhang. Hadamard product for low-rank bilinear pooling. *arXiv preprint arXiv:1610.04325*, 2016.

- [17] Zhou Yu, Jun Yu, Jianping Fan, and Dacheng Tao. Multi-modal factorized bilinear pooling with co-attention learning for visual question answering. *IEEE International Conference on Computer Vision (ICCV)*, pages 1839–1848, 2017.
- [18] Purushottam Kar and Harish Karnick. Random feature maps for dot product kernels. In *Artificial Intelligence and Statistics*, pages 583–591, 2012.
- [19] Yang Gao, Oscar Beijbom, Ning Zhang, and Trevor Darrell. Compact bilinear pooling. In *Proceedings of the IEEE conference on computer vision and pattern recognition*, pages 317–326, 2016.
- [20] Ninh Pham and Rasmus Pagh. Fast and scalable polynomial kernels via explicit feature maps. In *Proceedings of the 19th ACM SIGKDD international conference on Knowledge discovery and data mining*, pages 239–247. ACM, 2013.
- [21] Felix Xinnan X Yu, Ananda Theertha Suresh, Krzysztof M Choromanski, Daniel N Holtmann-Rice, and Sanjiv Kumar. Orthogonal random features. In *Advances in Neural Information Processing Systems*, pages 1975–1983, 2016.
- [22] Tamara G Kolda and Brett W Bader. Tensor decompositions and applications. *SIAM review*, 51(3):455–500, 2009.
- [23] Robb J Muirhead. *Aspects of multivariate statistical theory*, volume 197. John Wiley & Sons, 2009.
- [24] Colin Lea, Michael D. Flynn, Rene Vidal, Austin Reiter, and Gregory D. Hager. Temporal convolutional networks for action segmentation and detection. In *IEEE Conference on Computer Vision and Pattern Recognition (CVPR)*, pages 1003–1012, July 2017.
- [25] Yazan Abu Farha and Juergen Gall. Ms-tcn: Multi-stage temporal convolutional network for action segmentation. In *IEEE Conference on Computer Vision and Pattern Recognition (CVPR)*, 2019.
- [26] Sebastian Stein and Stephen J McKenna. Combining embedded accelerometers with computer vision for recognizing food preparation activities. In *Proceedings of the 2013 ACM international joint conference on Pervasive and ubiquitous computing*, pages 729–738. ACM, 2013.
- [27] Alireza Fathi, Xiaofeng Ren, and James M Rehg. Learning to recognize objects in egocentric activities. In *IEEE Conference On Computer Vision and Pattern Recognition (CVPR)*, pages 3281–3288. IEEE, 2011.
- [28] Yin Li, Zhefan Ye, and James M Rehg. Delving into egocentric actions. In *Proceedings of the IEEE Conference on Computer Vision and Pattern Recognition*, pages 287–295, 2015.
- [29] Diederik P Kingma and Jimmy Ba. Adam: A method for stochastic optimization. *arXiv preprint arXiv:1412.6980*, 2014.
- [30] Peng Lei and Sinisa Todorovic. Temporal deformable residual networks for action segmentation in videos. In *Proceedings of the IEEE Conference on Computer Vision and Pattern Recognition*, pages 6742–6751, 2018.

A Proof of Theorem 1

Proof. Let $R = 1$. Then, it follows from Eq.(5) and the property of an inner product of rank-one operators that

$$\begin{aligned}
k(\mathbf{z}_1, \mathbf{z}_2) &:= \langle \mathbf{z}_1, \mathbf{z}_2 \rangle = \langle \text{vec}(\mathbf{E}\mathbf{x}_1 \otimes \mathbf{F}\mathbf{y}_1), \text{vec}(\mathbf{E}\mathbf{x}_2 \otimes \mathbf{F}\mathbf{y}_2) \rangle_{\mathbb{R}^{MN}} \\
&= \sum_{i=1}^M \sum_{j=1}^N \langle \mathbf{e}_i, \mathbf{x}_1 \rangle \langle \mathbf{f}_j, \mathbf{y}_1 \rangle \langle \mathbf{e}_i, \mathbf{x}_2 \rangle \langle \mathbf{f}_j, \mathbf{y}_2 \rangle \\
&= \left(\sum_{i=1}^M \langle \mathbf{e}_i, \mathbf{x}_1 \rangle \langle \mathbf{e}_i, \mathbf{x}_2 \rangle \right) \left(\sum_{j=1}^N \langle \mathbf{f}_j, \mathbf{y}_1 \rangle \langle \mathbf{f}_j, \mathbf{y}_2 \rangle \right). \tag{12}
\end{aligned}$$

By virtue of [18, Lemma 2],

$$\mathbb{E}[k(\mathbf{z}_1, \mathbf{z}_2)] = MN \cdot \mathbb{E}_{\mathbf{e}}[\langle \mathbf{e}, \mathbf{x}_1 \rangle \langle \mathbf{e}, \mathbf{x}_2 \rangle] \mathbb{E}_{\mathbf{f}}[\langle \mathbf{f}, \mathbf{y}_1 \rangle \langle \mathbf{f}, \mathbf{y}_2 \rangle] = MN \langle \mathbf{x}_1, \mathbf{x}_2 \rangle \langle \mathbf{y}_1, \mathbf{y}_2 \rangle.$$

Now, suppose that $R > 1$. Then, we have

$$\begin{aligned}
k(\mathbf{z}_1, \mathbf{z}_2) &:= \langle \mathbf{z}_1, \mathbf{z}_2 \rangle = \left\langle \sum_{r=1}^R \text{vec}(\mathbf{E}^r \mathbf{x}_1 \otimes \mathbf{F}^r \mathbf{y}_1), \sum_{r=1}^R \text{vec}(\mathbf{E}^r \mathbf{x}_2 \otimes \mathbf{F}^r \mathbf{y}_2) \right\rangle_{\mathbb{R}^{MN}} \\
&= \sum_{r=1}^R \sum_{r'=1}^R \left\langle \text{vec}(\mathbf{E}^r \mathbf{x}_1 \otimes \mathbf{F}^r \mathbf{y}_1), \text{vec}(\mathbf{E}^{r'} \mathbf{x}_2 \otimes \mathbf{F}^{r'} \mathbf{y}_2) \right\rangle_{\mathbb{R}^{MN}} \\
&= \sum_{r=1}^R \sum_{r'=1}^R \left\langle \mathbf{E}^r \mathbf{x}_1, \mathbf{E}^{r'} \mathbf{x}_2 \right\rangle \left\langle \mathbf{F}^r \mathbf{y}_1, \mathbf{F}^{r'} \mathbf{y}_2 \right\rangle \\
&= \sum_{r=1}^R \sum_{r'=1}^R \left(\sum_{i=1}^M \langle \mathbf{e}_i^r, \mathbf{x}_1 \rangle \langle \mathbf{e}_i^{r'}, \mathbf{x}_2 \rangle \right) \left(\sum_{j=1}^N \langle \mathbf{f}_j^r, \mathbf{y}_1 \rangle \langle \mathbf{f}_j^{r'}, \mathbf{y}_2 \rangle \right). \tag{13}
\end{aligned}$$

Hence, it follows that

$$\begin{aligned}
\mathbb{E}[k(\mathbf{z}_1, \mathbf{z}_2)] &= \sum_{r=1}^R \sum_{r'=1}^R \left(\sum_{i=1}^M \mathbb{E}[\langle \mathbf{e}_i^r, \mathbf{x}_1 \rangle \langle \mathbf{e}_i^{r'}, \mathbf{x}_2 \rangle] \right) \left(\sum_{j=1}^N \mathbb{E}[\langle \mathbf{f}_j^r, \mathbf{y}_1 \rangle \langle \mathbf{f}_j^{r'}, \mathbf{y}_2 \rangle] \right) \\
&= \sum_{r=1}^R \left(\sum_{i=1}^M \mathbb{E}[\langle \mathbf{e}_i^r, \mathbf{x}_1 \rangle \langle \mathbf{e}_i^r, \mathbf{x}_2 \rangle] \right) \left(\sum_{j=1}^N \mathbb{E}[\langle \mathbf{f}_j^r, \mathbf{y}_1 \rangle \langle \mathbf{f}_j^r, \mathbf{y}_2 \rangle] \right) \\
&\quad + \sum_{r=1}^R \sum_{r'=r+1}^R \left(\sum_{i=1}^M \mathbb{E}[\langle \mathbf{e}_i^r, \mathbf{x}_1 \rangle \langle \mathbf{e}_i^{r'}, \mathbf{x}_2 \rangle] \right) \left(\sum_{j=1}^N \mathbb{E}[\langle \mathbf{f}_j^r, \mathbf{y}_1 \rangle \langle \mathbf{f}_j^{r'}, \mathbf{y}_2 \rangle] \right) \\
&= RMN \langle \mathbf{x}_1, \mathbf{x}_2 \rangle \langle \mathbf{y}_1, \mathbf{y}_2 \rangle \\
&\quad + \sum_{r=1}^R \sum_{r'=r+1}^R \left(\sum_{i=1}^M \gamma_i^r(\mathbf{x}_1) \gamma_i^{r'}(\mathbf{x}_2) \right) \left(\sum_{j=1}^N \xi_j^r(\mathbf{y}_1) \xi_j^{r'}(\mathbf{y}_2) \right),
\end{aligned}$$

where $\gamma_i^r(\mathbf{x}) := \mathbb{E}[\langle \mathbf{e}_i^r, \mathbf{x} \rangle]$ and $\xi_j^r(\mathbf{y}) := \mathbb{E}[\langle \mathbf{f}_j^r, \mathbf{y} \rangle]$. \square

B Proof of Corollary 1

Proof. Let $W_{ij} := \langle \mathbf{e}_i, \mathbf{x}_1 \rangle \langle \mathbf{e}_i, \mathbf{x}_2 \rangle \langle \mathbf{f}_j, \mathbf{y}_1 \rangle \langle \mathbf{f}_j, \mathbf{y}_2 \rangle$ for $i = 1, \dots, M$ and $j = 1, \dots, N$. For each W_{ij} , it follows from [18, Lemma 4] that

$$-p^2 f(p\tilde{R}^2)^2 \leq W_{ij} \leq p^2 f(p\tilde{R}^2)^2,$$

where we assume without loss of generality that $p \geq 1$ and $\tilde{R} \geq 1$. In our case, $f(x) = x$. Then, we have $-p^4 \tilde{R}^4 \leq W_{ij} \leq p^4 \tilde{R}^4$. Let $S_{MN} := \sum_{i=1}^M \sum_{j=1}^N W_{ij}$. We know that $\mathbb{E}[S_{MN}] = MN \langle \mathbf{x}_1, \mathbf{x}_2 \rangle \langle \mathbf{y}_1, \mathbf{y}_2 \rangle$. Then, it follows from Hoeffding's inequality that, for all $\epsilon > 0$,

$$\mathbb{P}(|S_{MN} - \mathbb{E}[S_{MN}]| \geq \epsilon) \leq 2 \exp\left(-\frac{\epsilon^2 MN}{2p^8 \tilde{R}^8}\right). \quad (14)$$

This concludes the proof. \square

C Proof of Theorem 2

Proof. Let $R = 1$. Then, we have $k(\mathbf{z}_1, \mathbf{z}_2) := \langle \mathbf{z}_1, \mathbf{z}_2 \rangle = (\langle \mathbf{E}^r \mathbf{x}_1, \mathbf{E}^r \mathbf{x}_2 \rangle)(\langle \mathbf{F}^r \mathbf{x}_1, \mathbf{F}^r \mathbf{x}_2 \rangle)$. Hence, with $\mathbf{E}^r = \frac{1}{\sigma^r} \mathbf{I}_{M \times D_X} \mathbf{R}^r \mathbf{P}^r$ and $\mathbf{F}^r = \frac{1}{\rho^r} \mathbf{I}_{N \times D_Y} \mathbf{S}^r \mathbf{Q}^r$, we have

$$\begin{aligned} \mathbb{E}[k(\mathbf{z}_1, \mathbf{z}_2)] &= \mathbb{E}[\langle \mathbf{E}^r \mathbf{x}_1, \mathbf{E}^r \mathbf{x}_2 \rangle] \mathbb{E}[\langle \mathbf{F}^r \mathbf{y}_1, \mathbf{F}^r \mathbf{y}_2 \rangle] \\ &= \exp\left(-\frac{\|\mathbf{x}_1 - \mathbf{x}_2\|_2^2}{2\sigma_r^2}\right) \exp\left(-\frac{\|\mathbf{y}_1 - \mathbf{y}_2\|_2^2}{2\rho_r^2}\right), \end{aligned}$$

where the last equality follows from [21, Theorem 1]. For $R > 1$, we have

$$k(\mathbf{z}_1, \mathbf{z}_2) := \langle \mathbf{z}_1, \mathbf{z}_2 \rangle = \sum_{r=1}^R \sum_{r'=1}^R \langle \mathbf{E}^r \mathbf{x}_1, \mathbf{E}^{r'} \mathbf{x}_2 \rangle \langle \mathbf{F}^r \mathbf{x}_1, \mathbf{F}^{r'} \mathbf{x}_2 \rangle.$$

Hence, with $\mathbf{E}^r = \frac{1}{\sigma^r} \mathbf{I}_{M \times D_X} \mathbf{R}^r \mathbf{P}^r$ and $\mathbf{F}^r = \frac{1}{\rho^r} \mathbf{I}_{N \times D_Y} \mathbf{S}^r \mathbf{Q}^r$, we have

$$\begin{aligned} \mathbb{E}[k(\mathbf{z}_1, \mathbf{z}_2)] &= \sum_{r=1}^R \sum_{r'=1}^R \mathbb{E}[\langle \mathbf{E}^r \mathbf{x}_1, \mathbf{E}^{r'} \mathbf{x}_2 \rangle] \mathbb{E}[\langle \mathbf{F}^r \mathbf{y}_1, \mathbf{F}^{r'} \mathbf{y}_2 \rangle] \\ &= \sum_{r=1}^R \mathbb{E}[\langle \mathbf{E}^r \mathbf{x}_1, \mathbf{E}^r \mathbf{x}_2 \rangle] \mathbb{E}[\langle \mathbf{F}^r \mathbf{y}_1, \mathbf{F}^r \mathbf{y}_2 \rangle] \\ &\quad + \sum_{r=1}^R \sum_{r'=r+1}^R \mathbb{E}[\langle \mathbf{E}^r \mathbf{x}_1, \mathbf{E}^{r'} \mathbf{x}_2 \rangle] \mathbb{E}[\langle \mathbf{F}^r \mathbf{y}_1, \mathbf{F}^{r'} \mathbf{y}_2 \rangle] \\ &= \exp\left(-\frac{\|\mathbf{x}_1 - \mathbf{x}_2\|_2^2}{2\sigma_r^2}\right) \exp\left(-\frac{\|\mathbf{y}_1 - \mathbf{y}_2\|_2^2}{2\rho_r^2}\right) \\ &\quad + \sum_{r=1}^R \sum_{r'=r+1}^R \mathbb{E}[\langle \mathbf{E}^r \mathbf{x}_1, \mathbf{E}^{r'} \mathbf{x}_2 \rangle] \mathbb{E}[\langle \mathbf{F}^r \mathbf{y}_1, \mathbf{F}^{r'} \mathbf{y}_2 \rangle] \end{aligned}$$

where the last equality follows from [21, Theorem 1]. This concludes the proof. \square

D Proof of Corollary 2

Proof. Assume that $R = 1$. Then we have

$$k(\mathbf{z}_1, \mathbf{z}_2) = \underbrace{\langle \mathbf{E}^r \mathbf{x}_1, \mathbf{E}^r \mathbf{x}_2 \rangle}_{U} \underbrace{\langle \mathbf{F}^r \mathbf{x}_1, \mathbf{F}^{r'} \mathbf{x}_2 \rangle}_{V}.$$

Since U and V are independent, we have

$$\text{Var}(k(\mathbf{z}_1, \mathbf{z}_2)) = \text{Var}(U)\text{Var}(V) + \text{Var}(U)(\mathbb{E}[V])^2 + \text{Var}(V)(\mathbb{E}[U])^2, \quad (15)$$

where

$$\begin{aligned} (\mathbb{E}[U])^2 &= (\mathbb{E}[\langle \mathbf{E}^r \mathbf{x}_1, \mathbf{E}^r \mathbf{x}_2 \rangle])^2 & (\mathbb{E}[V])^2 &= (\mathbb{E}[\langle \mathbf{F}^r \mathbf{y}_1, \mathbf{F}^r \mathbf{y}_2 \rangle])^2 \\ \text{Var}(U) &= \text{Var}(\langle \mathbf{E}^r \mathbf{x}_1, \mathbf{E}^r \mathbf{x}_2 \rangle) & \text{Var}(V) &= \text{Var}(\langle \mathbf{F}^r \mathbf{y}_1, \mathbf{F}^r \mathbf{y}_2 \rangle) \end{aligned}$$

It follows from [21, Theorem 1] that

$$(\mathbb{E}[U])^2 = \left(\exp \left(-\frac{\|\mathbf{x}_1 - \mathbf{x}_2\|_2^2}{2\sigma_r^2} \right) \right)^2, \quad (\mathbb{E}[V])^2 = \left(\exp \left(-\frac{\|\mathbf{y}_1 - \mathbf{y}_2\|_2^2}{2\rho_r^2} \right) \right)^2.$$

Let $a_r = \|\mathbf{x}_1 - \mathbf{x}_2\|_2^2/\sigma_r$ and $b_r = \|\mathbf{y}_1 - \mathbf{y}_2\|_2^2/\rho_r$. Then, by [21, Theorem 1], there exists a function f and g such that

$$\begin{aligned} \text{Var}(U) &\leq \frac{1}{2M} \left[\left(\left(1 - e^{-a_r^2}\right)^2 - \frac{M-1}{D_X} e^{-a_r^2} a_r^4 \right) + \frac{f(a_r)}{D_X^2} \right] \\ \text{Var}(V) &\leq \frac{1}{2N} \left[\left(\left(1 - e^{-b_r^2}\right)^2 - \frac{N-1}{D_Y} e^{-b_r^2} b_r^4 \right) + \frac{g(b_r)}{D_Y^2} \right]. \end{aligned}$$

Substituting everything back into (15) yields the result. \square